Nuclear resonance vibrational spectroscopy of a protein active-site mimic

2001 J. Phys.: Condens. Matter 13 7707

(http://iopscience.iop.org/0953-8984/13/34/315)

INSTITUTE OF PHYSICS PUBLISHING JOURNAL OF PHYSICS: CONDENSED MATTER

J. Phys.: Condens. Matter **13** (2001) 7707–7722 PII: S0953-8984(01)25013-9

Nuclear resonance vibrational spectroscopy of a protein active-site mimic

J T Sage[1], C Paxson[1], G R A Wyllie[2], W Sturhahn[3], S M Durbin[4], P M Champion[1], E E Alp[3] and W R Scheidt[2]

[1] Department of Physics and Center for Interdisciplinary Research on Complex Systems, Northeastern University, Boston, MA 02115, USA
[2] Department of Chemistry, Notre Dame University, Notre Dame, IN 46556, USA
[3] Advanced Photon Source, Argonne National Laboratory, Argonne, IL 60439, USA
[4] Department of Physics, Purdue University, West Lafayette, IN 47907, USA

E-mail: jtsage@neu.edu

Received 21 May 2001
Published 9 August 2001
Online at stacks.iop.org/JPhysCM/13/7707

Abstract

For many years, Mössbauer spectroscopy has been applied to measure recoilless absorption of x-ray photons by nuclei. Recently, synchrotron radiation sources have enabled the observation of weaker features separated from the recoilless resonance by the energy of vibrational quanta. This enables a form of vibrational spectroscopy with a unique sensitivity to the probe nucleus. Biological applications are particularly promising, because it is possible to selectively probe vibrations of a single atom at the active site of a complex biomolecule, while avoiding interference from the vibrations of thousands of other atoms. In contrast with traditional site-selective vibrational spectroscopies, nuclear resonance vibrational spectroscopy (NRVS) is not hampered by solvent interference and faces selection rule limitations only if the probe nucleus lies on a symmetry element. Here, we formulate a mathematical language appropriate for understanding NRVS measurements on molecular systems and apply it to analyse NRVS data recorded on ferrous nitrosyl tetraphenylporphyrin, Fe(TPP)(NO). This compound mimics the haem group found at the active site of many proteins involved in the biological usage of oxygen and nitric oxide. Measurements on such model compounds provide a baseline for evaluating the extent to which vibrations are localized at the active site of a protein, with the goal of elucidating the mechanisms of biological processes, such as intersite communication in allosteric proteins.

1. Introduction

It is a well-known consequence of energy conservation that absorption of a photon is accompanied by a change in the energy of the absorbing system by an amount equal to the energy of the photon. While momentum must also be conserved in this process, this fact does

not have significant consequences in most areas of spectroscopy. An important exception is the excitation of nuclear resonances, where the recoil energy $E_R = E_\gamma^2/2mc^2$ is very large, but the resonance linewidth is very narrow, reflecting the long lifetime of the nuclear excited state. For the $E_\gamma = 14.4$ keV resonance of ^{57}Fe, the recoil energy is 1.96 meV, while the linewidth is only 4.7 neV. Thus a simple analysis would seem to suggest that excitation of the nucleus would require a photon with an energy larger than the nuclear excited-state energy by an amount E_R, or conversely, that the energy of a photon emitted by an excited nucleus would have an energy smaller than the nuclear excited-state energy by an amount E_R.

However, in a celebrated experiment that won him the 1961 Nobel Prize in Physics, Rudolf Mössbauer demonstrated that a nucleus bound in a solid had a significant probability of absorbing or emitting a photon at an energy equal to the nuclear excited-state energy [1]. As he correctly concluded, this occurs because when the nucleus is in a bound state, its motion is quantized, and the nucleus can only change its vibrational energy by discrete amounts. In particular, there is a significant probability of absorbing with no change in vibrational state, at an energy equal to the energy of the nuclear excited state. Theorists quickly pointed out the corollary, that there should also be peaks displaced from the recoilless resonance by energies corresponding to vibrational quanta of the system [2, 3].

Two factors make it nearly impossible to observe these vibrational sidebands in a conventional Mössbauer experiment, which records the transmission of Doppler-shifted photons emitted by nuclei in a moving source. First, Doppler velocities of the order of hundreds of metres per second are needed to shift the energy of the emitted photon by an amount corresponding to typical vibrational quanta of the order of tens of meV [4]. A second, more fundamental, limitation stems from the fact that the resonance is now broadened by vibrational lifetimes, typically of the order of 1 meV. Thus, a strong vibrational sideband with an *integrated* cross section of the order of 1% of the recoilless resonance will have a *peak* cross section six to seven orders of magnitude weaker for a resonance with a linewidth of a few neV. With rare exceptions [4], there is little possibility of observing such a weak feature in a conventional transmission experiment.

Systematic experimental observations of nuclear absorption *with* recoil had to wait approximately 35 years for the development of suitable synchrotron sources [5, 6]. The unique properties of radiation from a third-generation synchrotron source circumvent these experimental limitations by enabling measurements in a time-resolved fluorescence excitation mode. The high source brilliance enabled the development of tunable monochromators with sub-meV resolution and acceptable output flux [7, 8]. The energy of the incident photons is tuned in the vicinity of the nuclear resonance, and the observed fluorescence signal is proportional to the number of photons absorbed by nuclei within the excited sample volume. The subnanosecond duration of the synchrotron pulse, together with fast detectors, allows the nuclear resonance signal to be distinguished from the background signal due to electronically scattered photons [9]. Electronically scattered photons arrive in coincidence with the pulse and are rejected, while fluorescence photons resulting from nuclear excitation (as well as photons scattered by the resonant nucleus, approximately 10% of the delayed signal for ^{57}Fe) arrive with a delay of the order of the nuclear lifetime (141 ns for ^{57}Fe).

Nuclear resonance vibrational spectroscopy (NRVS) has promise for elucidating the role of Fe in biology. Many physiologically essential proteins incorporate Fe, often at the centre of a planar haem group [10]. The best-known haem proteins (such as haemoglobin and cytochrome c oxidase) are involved in the transport and usage of molecular oxygen. Haem proteins also mediate the function of another diatomic molecule, nitric oxide (NO), a signalling molecule involved in diverse physiological processes including neurotransmission, immune function, and regulation of blood pressure [11, 12]. Both O_2 and NO bind to the Fe, and this atom is

believed to play a fundamental role in protein control of active-site reactivity. For example, motion of Fe into the plane of the haem plays a crucial role in the cooperative binding and transport of O_2 by haemoglobin [13, 14], while NO binding to guanylate cyclase severs the covalent connection of the Fe to the protein [15, 16], activating the enzyme [17]. Conventional Mössbauer studies provide insight into Fe dynamics in proteins [18–20], but only characterize the averaged fluctuations of the Fe nucleus. In contrast, NRVS resolves the contribution of individual vibrational modes to Fe fluctuations in proteins [21, 22].

The function of a protein often involves chemical reactions that take place at a localized site, and one approach to understanding protein behaviour is to synthesize and characterize small molecules that mimic the structure of this active site. Here, we present NRVS data on the compound ferrous nitrosyl tetraphenylporphyrin, Fe(TPP)(NO), a model for the active site of a haem protein, such as activated guanylate cyclase, with NO bound to the central Fe atom (figure 1). We formulate a multimode description of NRVS appropriate for molecular systems and apply it to characterize the vibrational motion of Fe in this compound. The approach used here does not depend on the feasibility of a direct simulation of the NRVS data from first principles [23], and is considerably more general than a formulation restricted to a single discrete mode [24]. Assuming only the harmonic approximation, we extract from NRVS data recorded on Fe(TPP)(NO) quantitative information on the composition and frequency of all modes involving significant Fe motion, which can be compared directly with the results of other experiments or calculations. The mode structure is much richer than previously observed for the O_2-binding haem protein myoglobin [22], probably reflecting the symmetry-lowering effect of the asymmetrically bound NO molecule. Quantitative analysis suggests that the haem doming coordinate, which is believed to couple to the binding of diatomic ligands, contributes to one or more of the observed low-frequency modes.

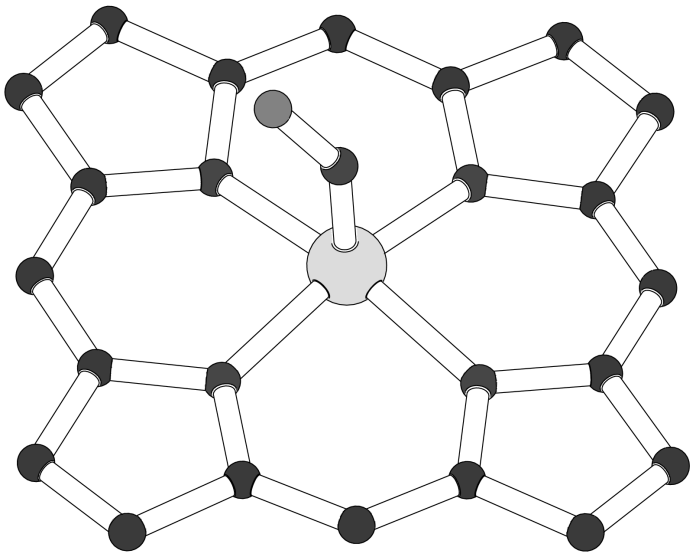

Figure 1. The structure of Fe(TPP)(NO), which mimics the active site of haem proteins. The Fe atom at the centre of the porphyrin is coordinated by the N atoms of four five-membered pyrrole rings. Note that the diatomic NO group bound to the Fe is tilted from the normal to the porphyrin plane, removing the fourfold degeneracy. For clarity, four phenyl groups, which bind to the methine carbons that bridge the pyrrole rings, have been omitted.

2. Background

2.1. The harmonic approximation and normal modes

The harmonic approximation describes the motion of nuclear centres of mass according to the Hamiltonian

$$\mathcal{H} = -\sum_{j=1}^{N} \frac{\hbar^2}{2m_j}\nabla_j^2 + \sum_{j=1}^{N}\sum_{k=1}^{N} \frac{1}{2}\vec{r}_j \cdot [\vec{\nabla}_j \vec{\nabla}_k V]_0 \cdot \vec{r}_k \tag{1}$$

where $\vec{r}_j$ is the displacement of atom j, with mass m_j, from its equilibrium position, $\vec{\nabla}_j$ is the gradient operator with respect to this coordinate, and derivatives of the potential energy function V are evaluated with all atoms at their equilibrium positions. Application of an appropriately chosen transformation

$$Q_\alpha = \sum_{j=1}^{N} \vec{e}_{j\alpha} \cdot \vec{r}_j \sqrt{m_j} \tag{2}$$

from mass-weighted Cartesian coordinates of the individual atoms to a set of normal coordinates Q_α leads to a decoupled representation of the Hamiltonian as a sum

$$\mathcal{H} = \sum_{\alpha=1}^{3N}\left(-\frac{1}{2}\hbar^2 \frac{\partial^2}{\partial Q_\alpha^2} + \frac{1}{2}\omega_\alpha^2 Q_\alpha^2\right) \tag{3}$$

of $3N$ one-dimensional harmonic oscillator Hamiltonians. The stationary states $|\{n_\alpha\}\rangle$ of this Hamiltonian, determined by a set $\{n_\alpha\}$ of occupation numbers for individual modes with frequencies ω_α, are direct products of the harmonic oscillator wavefunctions described in elementary quantum mechanics texts.

If the molecular potential V is known, numerical diagonalization of the Hessian matrix

$$\overleftrightarrow{\Omega}_{jk} = (m_j m_k)^{-1/2}[\vec{\nabla}_j \vec{\nabla}_k V]_0 \tag{4}$$

is computationally tractable even for proteins containing thousands of atoms. For an example of such a normal-mode calculation on myoglobin, see reference [25]. The dimensionless vectors $\vec{e}_{j\alpha}$ that describe this unitary transformation obey the normalization conditions

$$\sum_{j=1}^{N} e_{j\alpha}^2 = 1 \tag{5}$$

and

$$\sum_{\alpha=1}^{3N} e_{j\alpha}^2 = 3. \tag{6}$$

It is important to note that the latter sum extends over all $3N$ modes of the molecule, *including* modes of zero frequency (rotation and translation). The apparent difference in normalization of equations (5) and (6) reflects the association of three Cartesian coordinates with each atom. An alternative formulation of equation (6):

$$\sum_{\alpha=1}^{3N} (\vec{e}_{j\alpha} \cdot \hat{u})^2 = 1 \tag{7}$$

projects the vectors onto a molecule-fixed direction represented by the unit vector $\hat{u}$. We have previously used equation (7), together with symmetry arguments, to deduce the relative direction of motion of modes identified using NRVS in the protein deoxymyoglobin [22].

We shall see below that NRVS provides an absolute measurement of the mode composition factor $e_{j\alpha}^2$ if atom j has a suitable nuclear resonance, so it is important to understand its physical significance. The kinetic energies associated with atom j and mode α can be related using the expression $\vec{\nabla}_j = \sum_\alpha m_j^{1/2} \vec{e}_{j\alpha} (\partial/\partial Q_\alpha)$, which follows from the chain rule and equation (2). It is then straightforward to show that the kinetic energy added to the molecule by exciting mode α is partitioned among the individual atoms according to $e_{j\alpha}^2$; that is,

$$\Delta\langle -(\hbar^2/2m_j)\nabla_j^2 \rangle = e_{j\alpha}^2 \Delta\left\langle -\frac{1}{2}\hbar^2 (\partial/\partial Q_\alpha)^2 \right\rangle$$

(where $\Delta\langle\cdots\rangle$ represents the change in the expectation value of the enclosed operator in response to a change in the occupation number of mode α). Thus, the mode composition factor $e_{j\alpha}^2$ can be thought of as the fraction of mode kinetic energy associated with motion of atom j.

In special cases, this insight allows an expression for $e_{j\alpha}^2$ to be written by inspection. For example, it is apparent that

$$e_{j\alpha}^2 = \frac{m_j}{M} \tag{8}$$

is the mode composition factor for atom j, having mass m_j, for a translational mode of a molecule of total mass M. This expression also applies for pure acoustic lattice modes in a crystal where the total mass of the unit cell is M. Another simple case is a two-body oscillator composed of groups of atoms with total masses M_1 and M_2. Since the vibrational motion involves no translation of the centre of mass, it follows that the kinetic energy associated with motion of M_1 must be a fraction $M_2/(M_1 + M_2)$ of the total kinetic energy. Of this fraction, a subfraction m_j/M_1 is associated with the motion of an atom j that is included in M_1. Therefore,

$$e_{j\alpha}^2 = \frac{m_j}{M_1} \frac{M_2}{M_1 + M_2} \tag{9}$$

for a two-body oscillator.

The mode composition factor $e_{j\alpha}^2$ is also connected to the magnitude of atomic fluctuations. In a stationary state $|\{n_\alpha\}\rangle$ of a harmonic system, the mean square deviation of atom j from its equilibrium position may be expressed as a sum $\langle r_j^2 \rangle = \sum_\alpha' (2n_\alpha + 1)\langle r_{j\alpha}^2 \rangle_0$ over modes of non-zero frequency, where

$$\langle r_{j\alpha}^2 \rangle_0 = \frac{\hbar}{2m_j\omega_\alpha} e_{j\alpha}^2 \tag{10}$$

is the contribution of mode α to the zero-point fluctuations of atom j in the ground state. Thus, the mode composition factor $e_{j\alpha}^2$ is proportional to the contribution of mode α to the mean square fluctuations of atom j.

The traditional method for obtaining information on mode composition in bench-top vibrational spectroscopies (infrared and Raman) is to observe shifts in mode frequency when the mass of one or more atoms is altered by isotopic substitution. According to standard non-degenerate perturbation theory, a small change $\Delta\overleftrightarrow{\Omega}_{jk}$ in the Hessian matrix will shift mode frequencies according to the expression

$$\Delta(\omega_\alpha^2) = \sum_{jk} \vec{e}_{j\alpha} \cdot \Delta\overleftrightarrow{\Omega}_{jk} \cdot \vec{e}_{k\alpha} \tag{11}$$

to lowest order in $\Delta\overleftrightarrow{\Omega}_{jk}$. The perturbation caused by a small mass change can be estimated from the derivative

$$\frac{\mathrm{d}\overleftrightarrow{\Omega}_{jk}}{\mathrm{d}m_l} = -\left(\frac{1}{2m_l}\right)(\delta_{jl} + \delta_{kl})\overleftrightarrow{\Omega}_{jk} \tag{12}$$

as long as the mass change does not affect the potential V in equation (1). Substitution and use of the identity

$$\sum_j \vec{e}_{j\alpha} \cdot \overleftrightarrow{\Omega}_{jk} = \omega_\alpha^2 \vec{e}_{k\alpha}$$

leads to the result

$$\frac{\mathrm{d}(\ln \omega_\alpha)}{\mathrm{d}(\ln m_j)} = -\frac{1}{2} e_{j\alpha}^2. \tag{13}$$

At least in principle, then, frequency shifts in mode α resulting from isotopic substitution of atom j provide an estimate of the mode composition factor $e_{j\alpha}^2$. In practice, isotope shifts provide an important qualitative indicator of mode composition, but quantitative interpretation can be problematic because of the finite mass change, particularly if the frequency shift is comparable to the frequency separation from nearby modes. Moreover, substantial effort may be required to synthesize isotopically labelled forms of a complex molecule.

In contrast, NRVS provides an accurate means to directly determine *all* mode composition factors $e_{j\alpha}^2$ for the probe nucleus. For this reason, the above insights into the physical significance of the mode composition factors bear repeating:

- $e_{j\alpha}^2 \leqslant 1$ is the fraction of kinetic energy in mode α associated with motion of atom j;
- $e_{j\alpha}^2$ is proportional to the contribution of mode α to the mean square fluctuations of atom j;
- in simple cases, the frequency shift of mode α upon isotopic replacement of atom j is proportional to $e_{j\alpha}^2$.

2.2. Nuclear resonance vibrational spectroscopy (NRVS)

The absorption cross section

$$\sigma(E) = \frac{\pi}{2} \Gamma_0 \sigma_0 S(E - E_0) \tag{14}$$

for absorption of a photon of energy E and wave vector $\vec{k}$ with consequent excitation of a nuclear excited state can be expressed [3] in terms of a normalized excitation probability

$$S(E) = \sum_{if} p_i |\langle f| \exp(\mathrm{i}\vec{k} \cdot \vec{r}_j)|i\rangle|^2 \mathcal{L}_f[E - (E_f - E_i)] \tag{15}$$

which may be dominated by the recoilless line at $E = E_0$ (=14.413 keV for ^{57}Fe), but also includes features shifted from the resonance energy by the amount $E_f - E_i$ needed to excite the vibrational transition $i \longrightarrow f$. The peak cross section σ_0 and linewidth Γ_0 of the nuclear excitation are independent of the environment of the probe nucleus. A time-dependent reformulation

$$S(E) = \frac{1}{2\pi\hbar} \int_{-\infty}^{\infty} \mathrm{d}t \; \mathrm{e}^{\mathrm{i}Et/\hbar - \Gamma_0|t|/2\hbar} \langle \exp[-\mathrm{i}\vec{k} \cdot \vec{r}_j(0)] \exp[\mathrm{i}\vec{k} \cdot \vec{r}_j(t)] \rangle_T \tag{16}$$

of equation (15) in terms of a self-correlation function for the time-dependent position $\vec{r}_j(t)$ of the probe nucleus [3] often provides a more useful starting place for detailed calculations. The thermal average in equation (16) replaces the sum over states, with initial-state populations p_i, in equation (15).

Lipkin [26, 27] has elaborated a series of useful sum rules involving moments of the excitation probability $S(E)$. The lineshape functions $\mathcal{L}_f(E)$ appearing in equation (15) have unit area, $\int \mathcal{L}_f(E)\, \mathrm{d}E = 1$, so a simple closure argument ensures the normalization

$$\int_{-\infty}^{\infty} S(E)\, \mathrm{d}E = 1 \tag{17}$$

of the excitation probability. The first moment

$$\int_{-\infty}^{\infty} ES(E)\,\mathrm{d}E = E_R \tag{18}$$

of the excitation energy yields the recoil energy $E_R = \hbar^2 k^2/2m$ for a nucleus with mass m. The recoil energy E_R (=1.96 meV for ^{57}Fe) is independent of the environment of the probe nucleus. As a result, equation (18) provides an alternative normalization for experimental data that is more useful in practice [6] than equation (17). Higher moments provide model-independent values for various sorts of environment-specific information. In particular, the second moment

$$\int_{-\infty}^{\infty} E^2 S(E)\,\mathrm{d}E = E_R(4K_{av} + E_R) \tag{19}$$

yields the averaged kinetic energy K_{av} of the probe nucleus and is related to the second-order Doppler shift of the recoilless line observed in conventional Mössbauer spectroscopy [28].

2.2.1. Normal-mode formulation. In order to obtain more detailed information about the motion of the probe nucleus, it is necessary to introduce a model for the motion of the probe nucleus. The harmonic approximation summarized in section 2.1 allows a simple closed-form expression to be written for the area of each vibrational feature in $S(E)$. For molecular systems which contain discrete vibrational resonances, this formulation provides a convenient basis for comparison of experimental NRVS measurements with normal-mode calculations. According to equation (15), the normalized excitation probability

$$S(\bar{\nu}) = f\mathcal{L}_0(\bar{\nu}) + \sum_{\{\Delta n_\alpha\}} \phi_{\{\Delta n_\alpha\}} \mathcal{L}_v\left(\bar{\nu} - \sum_\alpha \Delta n_\alpha\, \bar{\nu}_\alpha\right) \tag{20}$$

for a harmonic system consists of a recoilless line with area fraction f, as well as a series of terms with area fraction $\phi_{\{\Delta n_\alpha\}}$ corresponding to changing the initial populations $\{n_\alpha\}$ of vibrational states by amounts $\{\Delta n_\alpha\}$. Here, we follow the usual practice in molecular spectroscopy and express the energy $E = hc\bar{\nu}$ or frequency $\omega_\alpha = 2\pi\bar{\nu}_\alpha$ in terms of the inverse free-space wavelength $\bar{\nu}$ of a photon with this energy or frequency.

Within the harmonic approximation, Zemach and Glauber [29] used the van Hove formulation (equation (16)) to calculate the fractional contribution

$$\phi_{\{\Delta n_\alpha\}} = f \prod_\alpha \left(\frac{\bar{n}_\alpha + 1}{\bar{n}_\alpha}\right)^{\Delta n_\alpha/2} I_{\Delta n_\alpha}(2z_{j\alpha}\sqrt{\bar{n}_\alpha(\bar{n}_\alpha + 1)}) \tag{21}$$

of the transition $\{n_\alpha\} \longrightarrow \{n_\alpha + \Delta n_\alpha\}$ to the normalized excitation probability $S(\bar{\nu})$. Here, the dimensionless quantity

$$z_{j\alpha} = \frac{\bar{\nu}_R}{\bar{\nu}_\alpha}(\hat{k}\cdot\vec{e}_{j\alpha})^2 \tag{22}$$

is expressed in terms of the nuclear recoil energy $E_R = hc\bar{\nu}_R = \hbar^2 k^2/2m_j$ and the unit vector $\hat{k} = \vec{k}/k$, and

$$\bar{n}_\alpha = \frac{1}{\exp(hc\bar{\nu}_\alpha/k_B T) - 1} \tag{23}$$

is the mean occupation number of mode α at temperature T. For ^{57}Fe, $\bar{\nu}_R = 15.8\ \mathrm{cm}^{-1}$. All transitions contribute to the recoilless fraction

$$f = \exp[-\langle(\vec{k}\cdot\vec{r}_{\mathrm{Fe}})^2\rangle_T] = \exp\left[-\sum_\alpha (2\bar{n}_\alpha + 1)z_{j\alpha}\right]. \tag{24}$$

In the low-temperature (high-frequency) limit $2\sqrt{\bar{n}_\alpha(\bar{n}_\alpha+1)}z_{j\alpha} \ll 1$, we can to a good approximation keep the leading term

$$I_n(x) = \left(\frac{1}{2}x\right)^{|n|} \Big/ |n|!$$

in the expansion of the modified Bessel function. In this limit, the 'recoil fraction' is

$$\phi = \frac{1}{3}\frac{\bar{\nu}_R}{\bar{\nu}_\alpha} e_{j\alpha}^2 (\bar{n}_\alpha + 1) f \tag{25}$$

for a fundamental transition $n_\alpha \longrightarrow n_\alpha + 1$. A similar expression with the factor $\bar{n}_\alpha + 1$ replaced by $\bar{n}_\alpha$ describes 'anti-Stokes' transitions $n_\alpha + 1 \longrightarrow n_\alpha$ appearing at energies $E = E_0 - hc\bar{\nu}_\alpha$. At the same level of approximation, the first overtone $n_\alpha \longrightarrow n_\alpha + 2$ contributes a fraction

$$\phi = \frac{1}{10}\left(\frac{\bar{\nu}_R}{\bar{\nu}_\alpha}\right)^2 e_{j\alpha}^4 (\bar{n}_\alpha + 1)^2 f \tag{26}$$

and a combination $n_\alpha \longrightarrow n_\alpha + 1$, $n_\beta \longrightarrow n_\beta + 1$ contributes a fraction

$$\phi = \frac{1}{15}(1 + 2\cos^2 \xi_{\alpha\beta}) \frac{\bar{\nu}_R^2}{\bar{\nu}_1 \bar{\nu}_2} e_{j\alpha}^2 e_{j\beta}^2 (\bar{n}_\alpha + 1)(\bar{n}_\beta + 1) f. \tag{27}$$

Both the recoil fractions ϕ and the recoilless fraction f depend on molecular orientation, as apparent from inspection of equations (21), (22), and (24). Equations (25)–(27) reflect an unweighted average over orientations, as appropriate for a solution or a polycrystalline sample. For a sample consisting of randomly oriented molecules, the needed averages are

$$\langle(\hat{k} \cdot \vec{e}_{j\alpha})^2\rangle = \frac{1}{3} e_{j\alpha}^2$$

$$\langle(\hat{k} \cdot \vec{e}_{j\alpha})^4\rangle = \frac{1}{5} e_{j\alpha}^2$$

$$\langle(\hat{k} \cdot \vec{e}_{j\alpha})^2 (\hat{k} \cdot \vec{e}_{j\beta})^2\rangle = e_{j\alpha}^2 e_{j\beta}^2 (1 + 2\cos^2 \xi_{\alpha\beta})/15$$

where $\xi_{\alpha\beta}$ is the angle between $\vec{e}_{j\alpha}$ and $\vec{e}_{j\beta}$. In principle, measurement of the intensity of combination modes would yield mode-specific information on the relative direction of motion of the probe nucleus.

The variation of the recoilless fraction f with molecular orientation is difficult to treat rigorously. The expressions for the recoil fractions ϕ in equations (25)–(27) result from simply replacing f with its isotropic average $\langle f \rangle$. Small systematic errors that might result from this neglect of the anisotropy of the recoilless fraction are minimized if f is close to unity. In section 4, we suggest a procedure to reduce such errors.

2.2.2. VDOS formulation. An alternative formulation [30] is particularly useful for a harmonic solid in which the normal modes form continuous phonon bands. In this case, it is natural to describe the NRVS signal in terms of a weighted vibrational density of states (VDOS)

$$D_j(\bar{\nu}) = \sum_\alpha (\hat{k} \cdot \vec{e}_{j\alpha})^2 \mathcal{L}(\bar{\nu} - \bar{\nu}_\alpha) \tag{28}$$

for atom j, since the individual frequencies are too close to resolve experimentally. The excitation probability

$$S(\bar{\nu}) = f\left[\mathcal{L}_0(\bar{\nu}) + \sum_{n=1}^{\infty} S_n(\bar{\nu})\right] \tag{29}$$

can be expanded in a series, where $S_n(E)$ represents the contribution of n-phonon processes. The one-phonon contribution

$$S_1(\bar{\nu}) = [\bar{n}(\bar{\nu}) + 1]\frac{\bar{\nu}_R}{\bar{\nu}} D_j(|\bar{\nu}|) \tag{30}$$

is proportional to the VDOS $D_j(E)$, and the n-phonon contribution

$$S_n(\bar{\nu}) = \frac{1}{n}\int \mathrm{d}\bar{\nu}'\, S_1(\bar{\nu}')S_{n-1}(\bar{\nu} - \bar{\nu}') \tag{31}$$

is a convolution of the one-phonon and $(n-1)$-phonon contributions.

While formally equivalent to the above formulation in terms of normal modes (section 2.2.1), the VDOS formulation given in equations (28)–(31) is often more useful for a crystalline solid. In particular, an iterative procedure [6] based on equation (31) directly extracts $D(\bar{\nu})$ from the measured $S(\bar{\nu})$, after subtraction of the recoilless line. This is a valuable feature for systems where $D(\bar{\nu})$ is continuous, since multiphonon contributions will in general not be spectrally resolved from one-phonon contributions in the observed $S(\bar{\nu})$.

The preceding expressions are rigorous for an oriented harmonic crystal. However, the effect of orientational averaging must be considered for unoriented polycrystalline samples. In particular, since $\langle S_1(\bar{\nu}')S_{n-1}(\bar{\nu} - \bar{\nu}')\rangle \neq \langle S_1(\bar{\nu}')\rangle\langle S_{n-1}(\bar{\nu} - \bar{\nu}')\rangle$ in general [28], use of equation (31) to estimate the multiphonon contributions may lead to systematic errors in the iteratively extracted VDOS. In general, measurement of $S(\bar{\nu})$ at a single temperature may not uniquely determine $D(\bar{\nu})$ without additional information about vibrational anisotropy. However, iterative extraction of $D(\bar{\nu})$ is still rigorously correct if vibrational motion is isotropic, as in a cubic crystal [6], and the systematic errors are expected to be small for simple crystals, where vibrational anisotropy is modest. Significantly larger lattice mode anisotropy might be expected for the molecular crystal under investigation here.

3. Methods

^{57}Fe-enriched Fe(TPP)Cl was prepared using the metallation procedure described by Landergren and Baltzer [31]. Fe(TPP)(NO) was then prepared by a route based upon the synthetic method of Scheidt and Frisse [32]. Fe(TPP)Cl was dissolved in a small volume of chloroform, methanol and pyridine were added, and nitric oxide was bubbled through the solution for several minutes. The product was then precipitated by addition of a large volume of methanol, isolated by filtration upon sintered glass, and washed with several portions of methanol. The resulting polycrystalline powder was mixed with minimal Apiezon N grease for binding, loaded into a milled depression in a sapphire block, and covered with a Mylar sheet. The sapphire block was then mounted on the cold finger of a cryostat with Mylar windows.

Measurements were performed at sector 3-ID-D of the Advanced Photon Source at Argonne National Laboratory. A high-resolution x-ray monochromator [8] tuned the energy of the x-ray beam in the vicinity of the 14.4 keV resonance of ^{57}Fe with a resolution of approximately 7 cm^{-1}. K fluorescence emitted by excited ^{57}Fe nuclei was detected using a large-area APD detector. Pulses from the APD were recorded by a counter that was enabled after a delay to discriminate the 6.4 keV fluorescence photons from the large background of electronically scattered 14.4 keV photons, which arrive in coincidence with the x-ray pulse. The spectrum shown in figure 2 is a sum of ten scans, in each of which counts were recorded for 5 s every 0.2 meV while scanning the incident x-ray energy.

4. Results

The recoilless line at $E = E_0$ dominates the measured spectrum of ^{57}Fe(TPP)(NO) at 80 K (figure 2). Well-resolved peaks at higher energy indicate excitation of discrete vibrational modes coincident with x-ray absorption by the ^{57}Fe nucleus. There is significant thermal excitation of low-frequency vibrational modes at this temperature, and a peak visible 130 cm^{-1} below the recoilless line in figure 2 corresponds to de-excitation of the same mode responsible for the peak 130 cm^{-1} above the recoilless line. The area ratio $(\bar{n}_\alpha + 1)/\bar{n}_\alpha = \exp(hc\bar{\nu}_\alpha/k_BT)$ of these two features provides a value $T = 80$ K for the sample temperature. Although most of the spectrum shows little indication of dispersion, acoustic phonons obviously involve motion of ^{57}Fe and presumably contribute to the unresolved features on the shoulder of the recoilless line. Note that the experimental resolution (0.85 meV $\simeq$ 7 cm^{-1}) is comparable to vibrational lifetime broadening, but many orders of magnitude larger than the intrinsic 4.7 neV nuclear linewidth. As a result, the peak cross sections for the vibrational features in figure 2 are more than 10^7 times weaker than the recoilless line, contrary to what might be concluded from a cursory examination of the data.

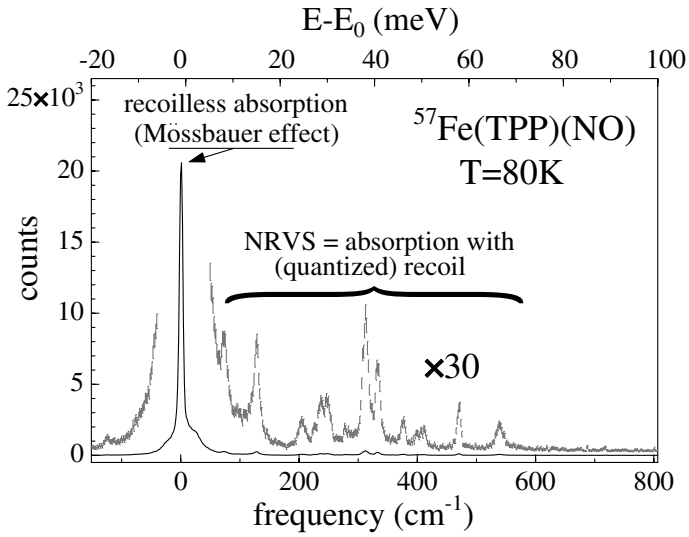

Figure 2. The NRVS signal recorded from polycrystalline ^{57}Fe(TPP)(NO) at $T = 80$ K. The temperature was estimated by equating the ratio of the features at ± 130 cm^{-1} to the Boltzmann factor $\exp\{-hc\bar{\nu}/k_BT\}$.

Figure 3 shows the experimental spectrum of polycrystalline ^{57}Fe(TPP)(NO) after normalization so that the first moment yields the recoil energy $\bar{\nu}_R$, as required by Lipkin's sum rule (equation (18)) [26, 27]. The resulting normalized spectrum is proportional to $S(\bar{\nu})$ for energies that are sufficiently separated from the recoilless line. Table 1 lists frequencies and recoil fractions resulting from fitting the normalized spectrum to a sum of Lorentzians. According to equation (25), experimental values for the mode composition factors e^2_{Fe} can be determined from the areas of the corresponding one-quantum features in the excitation probability, given a value for the recoilless fraction f. However, the limited experimental resolution presents some practical difficulties in determining the latter quantity, because the recoilless line is not cleanly resolved from the distribution of unresolved vibrational states that contribute shoulders on the central resonance in figure 2.

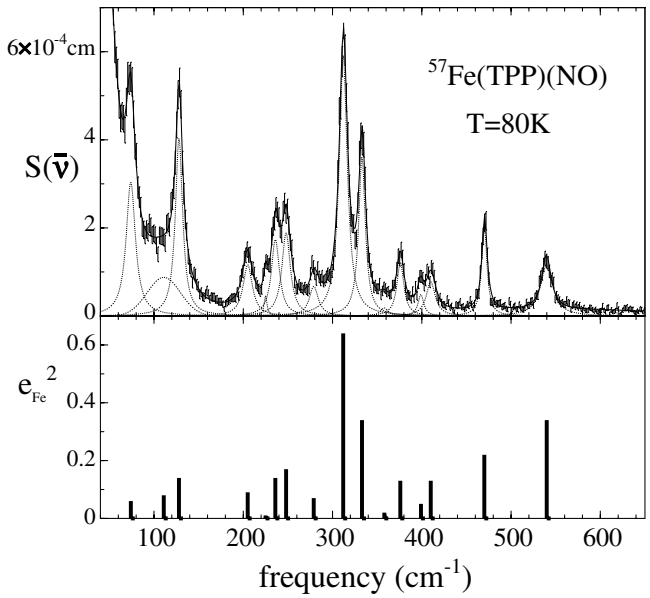

Figure 3. Upper panel: the excitation probability derived from experimental data on Fe(TPP)(NO) shown in figure 2. Dashed curves represent the results of a fit of the excitation probability to a series of Lorentzian peaks. Lower panel: mode composition factors derived from equation (25), using the fitted peak areas from the upper panel.

Elsewhere [33], this issue has been successfully dealt with by assuming a Debye frequency distribution and extrapolating through $E = E_0$ to determine the underlying vibrational contribution, with the remaining fraction attributed to recoilless absorption. The resulting values for the recoilless fraction agree well with those determined using conventional Mössbauer measurements [33]. Here, our primary goal is to determine accurate values for the mode composition factors, and we adopt an alternative approach.

We estimate a value $f' = 1 - \sum' \phi$ by summing *only* over the resolved features listed in table 1, which we successfully fit to symmetric peaks, finding $f' = 0.948$. The mode composition factors $e^2_{\rm Fe}$ in table 1 are then calculated by inverting equation (25), using this value for f' and the experimental recoil fractions ϕ. Table 1 also lists values for the contributions of individual modes to the zero-point fluctuations of the Fe, as calculated from equation (10). (Here and below, we take $j =$ Fe and suppress the mode index α that appears explicitly in equations (10) and (25).) Two tests suggest that the resulting values for $e^2_{\rm Fe}$ are accurate. First, the value of f' calculated independently from equation (24), using the frequencies and $e^2_{\rm Fe}$-values listed in table 1, yields a consistent value $f' = \exp[-\frac{1}{3}\sum'(\bar\nu_R/\bar\nu)(2\bar n+1)e^2_{\rm Fe}] = 0.944$. A more convincing test compares the value

$$\bar K = \frac{1}{12}\sum{}' \bar\nu(2\bar n + 1)e^2_{\rm Fe} \tag{32}$$

for the mean kinetic energy of the Fe nucleus calculated from our harmonic model, yielding $\bar K = 74\ {\rm cm}^{-1}$, with the model-independent value

$$\bar K = \frac{\langle \bar\nu^2\rangle - \bar\nu_R^2}{4\bar\nu_R} \tag{33}$$

determined from Lipkin's sum rule (equation (19)) [26, 27], yielding $\bar K = 76\ {\rm cm}^{-1}$. (The spectral moment in equation (33) is defined as $\langle \bar\nu^n\rangle = \int \bar\nu^n S(\bar\nu)\ {\rm d}\bar\nu$.) Since the former

Table 1. Mode composition analysis for Fe(TPP)(NO) at $T = 80$ K.

Frequency (cm^{-1})	FWHM (cm^{-1})	Recoil fraction $\times 10^3$	e^2_{Fe}	$\langle r^2_{Fe}\rangle_0$ (pm^2)
74	12.6	6.0	0.06	2.6
111	43.9	4.1	0.08	2.1
128	9.8	6.2	0.14	3.3
205	12.6	2.3	0.09	1.3
225	4.2	0.3	0.01	0.2
236	11.0	3.0	0.14	1.7
248	11.5	3.4	0.17	2.0
279	12.3	1.3	0.07	0.7
312	11.0	10.2	0.64	6.1
333	9.0	5.1	0.34	3.0
358	10.4	0.3	0.02	0.2
376	9.4	1.8	0.13	1.1
399	7.8	0.6	0.05	0.4
410	12.3	1.5	0.13	0.9
470	7.3	2.3	0.22	1.4
540	16.9	3.1	0.34	1.8
		$1 - \sum' \phi = 0.948$	$\sum' e^2_{Fe} = 2.62$	

value is dominated by frequencies above 300 cm^{-1}, the agreement of these two independent values gives confidence that the e^2_{Fe}-values reported in table 1 do not suffer from a significant systematic error due to misestimation of f'.

Note that the quantity f' is simply an intermediate stage in the determination of the mode composition factors e^2_{Fe}, and should *not* be interpreted as the true recoilless fraction that would be measured in a conventional high-resolution Mössbauer experiment. In fact, by subtracting the resolution function from $S(\bar{\nu})$ to obtain a result that is approximately flat near $\bar{\nu} = 0$ and equating the area of the remaining spectrum to $1 - \langle f\rangle$, we roughly estimate a much smaller value $\langle f\rangle = 0.72$ for the orientationally averaged recoilless fraction. In fact, it is apparent from the experimental data in figure 2 that the low-frequency shoulders are a much larger fraction of the spectral area than the discrete modes listed in table 1, and will dominate the value of the recoilless fraction measured in a conventional Mössbauer experiment.

The reason that this procedure works reasonably well can be seen from the VDOS formulation of $S(\bar{\nu})$. Because each term in the expansion takes the form of a convolution of the previous term with the first-order term (equation (31)), each peak in the spectrum should in principle exhibit asymmetric shoulders similar to those apparent on examination of the recoilless line (figure 2). However, the shoulders on the wings of the individual vibrational peaks will vary from peak to peak, depending on the direction of Fe motion in each individual mode. In the experimental spectrum, these asymmetric shoulders are not apparent on the vibrational peaks. This presumably results from the broader linewidth of these features, compared to the recoilless line, and the limited signal-to-noise ratio. Nevertheless, the fit accurately reproduces the entire spectral area, and since the shoulders constitute a significant fraction of this area, the sharp peaks in the fitting function must include the area of the asymmetric shoulders. As a result, it should be approximately correct to reformulate the expansion (equation (29)) so that the zeroth-order contribution has the form not of a delta function, but of the spectrum that would be observed due only to the continuous part of the density of states responsible for the low-frequency shoulders. Sharp features due to the discrete part of the density of states then appear in first and higher orders of the expansion, and the 'nearly recoilless fraction' f' is calculated from the right-hand side of equation (24) by

summing only over discrete modes. Note that if, as here, the vibrational subspace is partitioned so that f' is significantly closer to unity than f, this procedure should reduce the severity of the approximation of neglecting the anisotropy of the recoilless fraction.

More formally, we may partition the vibrational degrees of freedom into a subspace (with occupation numbers $\{n_\alpha\}$) that contributes to the sharp vibrational resonances and a second subspace (with occupation numbers $\{n_\beta\}$) whose fundamental transitions are not clearly resolved from the recoilless line. Then we combine the area of each vibrational feature in the spectrum defined by a set of occupation numbers $\{\Delta n_\alpha\}$ (including the recoilless resonance with $\{\Delta n_\alpha = 0\}$) with the areas of features associated with all possible simultaneous excitations $\{\Delta n_\beta\}$ of the $\{n_\beta\}$ subspace. The subspace partitioning allows us to factor the contribution of the $\{n_\beta\}$ subspace out of the product in equation (21), so that the total area

$$\phi'_{\{\Delta n_\alpha\}} = \sum_{\{\Delta n_\beta\}} \phi_{\{\Delta n_\beta;\Delta n_\alpha\}}$$

of the resolved resonance is easily shown to retain the form of equation (21), with f replaced by

$$f' = \sum_{\{\Delta n_\beta\}} \phi_{\{\Delta n_\beta;\Delta n_\alpha=0\}} > f.$$

5. Discussion

A striking feature of the NRVS data on ^{57}Fe(TPP)(NO) is the large number of well-resolved vibrational resonances. These sharp features contrast with the broad phonon bands observed for simpler crystalline systems such as Fe metal and oxides [6, 33], reflecting the reduced dispersion characteristic of molecular solids. The number of modes is significantly larger than the number observed in NRVS data from ^{57}Fe-enriched myoglobin [22]. The reduced symmetry of the Fe environment brought about by asymmetric binding of the NO ligand is likely to contribute to activating these modes. In addition to the tilted orientation of the bound NO ligand, both high-resolution x-ray structures [34] and recent DFT calculations [35] on five-coordinate nitrosyl iron porphyrins reveal that the in-plane Fe–N_{pyr} bonds are significantly shorter in the direction of the NO tilt. In the absence of the axial NO ligand, the Fe lies on a centre of D_{4h} symmetry, and all Fe motion will involve modes of A_{2u} (out-of-plane) or E_u (in-plane) symmetry. NO binding removes this restriction and frees the Fe to participate in a wider range of vibrational motions. Other factors that might restrict the number of modes identified in myoglobin NRVS data include changes in the peripheral groups attached to the porphyrin skeleton, interactions with the polypeptide, and the limited signal-to-noise ratio of the protein data.

The results in table 1 present an important new challenge for theoretical calculations. Traditional vibrational spectroscopies, such as infrared and Raman, typically provide frequencies for a restricted subset of modes that modulate electronic properties of the molecule [36]. NRVS not only identifies the frequencies of *all modes with significant Fe motion*, but also provides quantitative information on mode composition that an accurate calculation must reproduce. Most of the modes observed here are not seen in Raman spectra of Fe(TPP)(NO) derivatives in solution at room temperature [37]. In fact, there are no precise frequency correspondences. In particular, ^{14}NO/^{15}NO isotope shifts and DFT calculations associate 65% Fe–NO stretching character with a mode observed at 524 (527) cm^{-1} for Fe(TPP)(NO) in benzene (dichloromethane) solution [37]. The nearest frequency that we observe in polycrystalline Fe(TPP)(NO) at 80 K is 540 cm^{-1}. The value $e^2_{Fe} = 0.34$ observed here compares

well with the value $e^2_{Fe} = 0.31$ predicted by equation (9) for a two-body Fe–NO oscillator, and it is likely that Fe–NO stretching remains a dominant contribution for the 540 cm^{-1} mode. However, intermolecular interactions in the crystalline environment may alter its frequency or detailed composition. Temperature-dependent structural changes cannot be excluded. Also of interest are the pair of modes at 312 cm^{-1} and 333 cm^{-1}, which have the largest e^2_{Fe}-values other than those of the 540 cm^{-1} mode. These modes may be analogous to the in-plane Fe–N_{pyr} modes that dominate the spectrum of photolysed myoglobin. However, the unequal e^2_{Fe}-values in Fe(TPP)(NO) contrast with the nearly equal values observed for myoglobin [22]. It is conceivable that this asymmetry reflects interactions with another mode or modes, such as the Fe–N–O bending mode, which also involves in-plane Fe motion. Normal-mode calculations will shed more light on the character of these modes.

The value $\sum' e^2_{Fe} = 2.62$ obtained by summing only over the modes listed in table 1 is quite close to the value $3 - 3m_{Fe}/M = 2.72$ that would result from excluding acoustic modes (equation (8)) from the sum in equation (6). This result further validates the method introduced here to determine values for e^2_{Fe}. Moreover, it suggests a clean partitioning of the ^{57}Fe NRVS spectrum into discrete modes, which resemble vibrations of the isolated molecule, and acoustic phonon bands, which give rise to the broad feature visible below ~30 cm^{-1} on the shoulders of the recoilless resonance (figure 2). These acoustic phonons also make the dominant contribution to the recoilless fraction $f = 0.72$ estimated above. A more detailed quantitative analysis of the acoustic phonons would have to take into account the highly anisotropic motion expected on the basis of the parallel packing of the planar porphyrin molecules into the lattice.

One important motivation for NRVS investigations of haem proteins and model compounds is to identify and characterize modes that participate in biochemical reactions. In particular, the O_2 binding reaction in myoglobin and haemoglobin involves Fe motion perpendicular to the haem plane [13, 14]. DFT calculations on isolated haems predict the frequency of this haem 'doming' mode to lie in the range [38] of 50–70 cm^{-1}. Photochemical release of NO from myoglobin with a femtosecond laser pulse leads to coherent oscillations with 40 cm^{-1} and 80 cm^{-1} frequencies [39, 40], but does not provide direct information on the atoms involved in the motion. NRVS data on myoglobin failed to identify a well-resolved mode with the intensity expected for a haem doming mode in this frequency region. The proposed explanation is that the protein environment fundamentally alters the character of the doming mode, with the result that atomic motion throughout the protein is involved and the fraction of mode energy invested in Fe motion is consequently reduced [22].

Since the analysis presented above for Fe(TPP)(NO) appears to account for all intramolecular vibrations with significant Fe motion, one or more of the observed modes must involve the haem doming coordinate. The largest e^2_{Fe}-value reported here for modes below 200 cm^{-1} is for the 128 cm^{-1} mode, This frequency is significantly higher than the 40 cm^{-1} frequency observed following NO photolysis from myoglobin [40], or the 50–70 cm^{-1} region identified in calculations on a porphyrin with an unligated four-coordinate Fe [38]. Although there is a mode near the expected frequency range, at 74 cm^{-1}, its e^2_{Fe}-value is much smaller than the value $e^2_{Fe} \simeq 0.3$ previously estimated [22] for the haem doming mode. Clearly, caution is required, since the asymmetry induced by NO binding may introduce a significant component of Fe motion into low-frequency porphyrin modes such as 'saddling', which would involve no Fe motion in the strict D_{4h} symmetry of a four-coordinate porphyrin. Moreover, some frequency differences are not unexpected, due to variations in Fe ligation, porphyrin type, and environment (polypeptide, crystal lattice, or vacuum). Normal-mode calculations will be needed to evaluate the contribution of haem doming to the low-frequency modes observed here for Fe(TPP)(NO).

Since the haem doming coordinate is directly involved in the oxygen-binding reaction, there is particular interest in determining whether the mode remains localized at the haem when placed in the protein environment, or whether it acquires a more global character, involving the motion of atoms distant from the haem. In order to understand the mechanism of site-to-site communication in allosteric proteins and other biomolecules, it is crucial to establish whether biochemical reactions at an active site directly involve the motion of atoms at distant sites on vibrational timescales or whether intersite communication primarily results from a slower readjustment of the global protein conformation to a rapid structural change at the active site. Successful identification of the haem doming mode in a model compound would open an avenue of investigation aimed at characterizing this reaction coordinate in a protein. In particular, determination of e^2_{Fe} for a localized doming mode in a haem model compound would provide a more definitive baseline value for comparison with NRVS measurements on haem proteins. As we discuss elsewhere [22], NRVS provides a unique *experimental* probe of mode localization, a crucial issue that previously could only be addressed theoretically.

Acknowledgments

We acknowledge financial support from NIH GM-52002 (JTS), NIH DK-35090 (PMC), NSF 99-83100 and 99-04516 (JTS and PMC), DOE DE-F602-96-ER45581A (SMD), and NIH GM-38401 (WRS). Use of the Advanced Photon Source was supported by the US Department of Energy, Basic Energy Sciences, Office of Science, under Contract No W-31-109-Eng-38.

References

[1] Mössbauer R L 1958 *Z. Phys.* **151** 124
[2] Visscher W M 1960 *Ann. Phys., NY* **9** 194
[3] Singwi K S and Sjölander A 1960 *Phys. Rev.* **120** 1093
[4] Weiss H and Langhoff H 1979 *Phys. Lett.* A **69** 448
[5] Seto M *et al* 1995 *Phys. Rev. Lett.* **74** 3828
[6] Sturhahn W *et al* 1995 *Phys. Rev. Lett.* **74** 3832
[7] Toellner T S *et al* 1997 *Appl. Phys. Lett.* **71** 2112
[8] Toellner T S 2000 *Hyperfine Interact.* **125** 3
[9] Sturhahn W *et al* 1996 *Nucl. Instrum. Methods* A **372** 455
[10] Lindley P F 1996 *Rep. Prog. Phys.* **59** 867
[11] Snyder S H and Bredt D S 1992 *Sci. Am.* **266** 68
[12] Ignarro L J *et al* 1999 *J. Cardiovasc. Pharmacol.* **34** 879
[13] Hoard J L *et al* 1965 *J. Am. Chem. Soc.* **87** 2312
[14] Perutz M F 1970 *Nature* **228** 726
[15] Yu *et al* 1994 *J. Am. Chem. Soc.* **116** 4117
[16] Stone *et al* 1995 *Biochem. Biophys. Res. Commun.* **207** 572
[17] Zhao Y *et al* 2000 *Proc. Natl Acad. Sci. USA* **96** 14753
[18] Parak F and Formanek H 1971 *Acta Crystallogr.* A **27** 573
[19] Keller H and Debrunner P G 1980 *Phys. Rev. Lett.* **45** 68
[20] Parak F and Knapp E W 1984 *Proc. Natl Acad. Sci. USA* **81** 7088
[21] Keppler C *et al* 1997 *Eur. Biophys. J.* **25** 221
[22] Sage J T *et al* 2001 *Phys. Rev. Lett.* **86** 4966
[23] Paulsen H *et al* 1999 *Phys. Rev.* B **59** 975
[24] Knapp E W *et al* 1997 *Molecular Modelling and Dynamics of Bio-Organic Systems* (Amsterdam: Kluwer Academic) p 319
[25] Melchers B *et al* 1996 *Biophys. J.* **70** 2092
[26] Lipkin H J 1962 *Ann. Phys., NY* **18** 182
[27] Lipkin H J 1995 *Phys. Rev.* B **52** 10 073
[28] Sturhahn W and Chumakov A 2000 *Hyperfine Interact.* **123+124** 809

[29] Zemach A C and Glauber R J 1956 *Phys. Rev.* **101** 118
[30] Sturhahn W and Kohn V G 2000 *Hyperfine Interact.* **123+124** 367
[31] Landergren M and Baltzer L 1990 *Inorg. Chem.* **29** 556
[32] Scheidt W R and Frisse M E 1975 *J. Am. Chem. Soc*. **97** 17
[33] Chumakov A I *et al* 1996 *Phys. Rev.* B **54** R9596
[34] Scheidt W R *et al* 2000 *J. Am. Chem. Soc.* **122** 4651
[35] Ghosh A and Wondimagegn T 2000 *J. Am. Chem. Soc*. **122** 8101
[36] Parak F and Achterhold K 1999 *Hyperfine Interact.* **123+124** 825
[37] Vogel K M *et al* 1999 *J. Am. Chem. Soc.* **121** 9915
[38] Kozlowski P *et al* 1998 *J. Phys. Chem.* B **102** 2603
[39] Zhu L *et al* 1994 *Science* **266** 629
[40] Rosca F *et al* 2000 *J. Phys. Chem.* A **104** 4280